On the survivability of WECs through submergence and passive controllers

Elie Al Shami, Alexandre Pichard, Mathieu Cocho, Ian Gough and Miguel Santos Herran

Abstract—**The survivability of WECs during extreme seas and heavy storms has proven to be challenging during the deployment of devices as they often fail during extreme storms. The survival mechanism is often inherited with the device design and mode of operation. It is not economically and logistically viable for devices to be taken back onshore in case of storms. Some devices lock their PTOs during heavy storms and others lock all the moving parts all together, in the case of CETO, its design has an advantage where it can be submerged. CETO is a buoyant actuator WEC composed of a buoy submerged close to the surface. Three tethers connect CETO to the sea-bottom through rotary PTOs, allowing the device to be wound down, submerged, and therefore, less exposed to the extreme loads at the sea surface during large storms. This paper will study the survivability of the device during extreme sea-states and will examine the required depth to bring its response back to operational conditions. This work will also look at the alteration of some passive controllers, such as a conventional spring to minimize the response of the device instead of maximising the power capture. With the PTO objective altered in extreme sea-states to minimize the response instead of capturing power, the possibility of harvesting power during extreme sea-states with the device submerged will be checked. Finally, the survivability strategy of CETO through submergence will be showcased with wave tank experiments conducted at IHC as part of the Europewave program. This work will focus on solving the fundamental challenge of wave energy by reducing the peak to average design parameters.**

Keywords—control, **extreme conditions, hydrodynamics, survivability, wave tank, WEC**

I. Introduction

WAVE energy converters (WECs) have been bridging the gap between research and development and full scale deployment and commercialisation [1]. However, the harsh marine environment presents significant challenges to the survivability and reliability of WECs [2], which can impact their economic viability and practical feasibility.

The survivability of WECs depends on various factors, such as the design and construction of the device, the survivability strategy used, the operating conditions, and the extreme wave loads. The survivability is often evaluated through reliability and availability analyses [3], [4], which consider the failure modes, repair times, and downtime of the WECs.

While many studies have focused on the performance and efficiency of WECs [5], [6], fewer studies have investigated their survivability and risk of failure [7]. There is plenty of work conducted regarding the modelling of WECs in extreme sea-states. CFD (Computational Fluid Dynamics) numerical models of a WECs were formulated in [8], [9], and [10] and used to simulate the response of WECs in extreme and irregular waves. Methods to statistically model and characterize extreme waves and loads in order to simulate WECs under extreme waves were formulated in [3], [11], [12].

However, the literature lacks methods which suggest survivability modes for WECs and assumes that the devices can be designed in order to sustain the loads of extremes waves. If EMEC (European Marine Energy Centre) location was used as an example [13], a WEC that can potentially be placed there has to be designed based on the highest waves in a 50-year return period. The wave energy flux of the most occurring sea-state at EMEC is 1% of the wave energy flux of the largest wave in the 50-year return contour for the same site. Hence, it's unreasonable to design any of the system components to sustain loads that are substantially larger than the operational loads, and a survival strategy should be developed that can progress

This work is part of the Europewave project that has received funding from the European Union's Horizon 2020 research and innovation Programme under grant agreement No 883751

Elie Al Shami is a hydrodynamics engineer working for CWEI (Carnegie Wave Energy Ireland) located in Bilbao, Spain. E-mail: ealshami@carnegiece.com

Alexandre Pichard is the CTO at Carnegie.

Miguel Santos Herran is a project manager for CWEI (Carnegie Wave Energy Ireland) handling the Europewave project and is located in Spain.

Ian Gough is an electrical engineer for CWEI (Carnegie Wave Energy Ireland) working on the Europewave project and is located in Spain.

Mathieu Cocho is a data analysist engineer working for Carnegie.

Digital Object Identifier: https://doi.org/10.36688/ewtec-2023-298

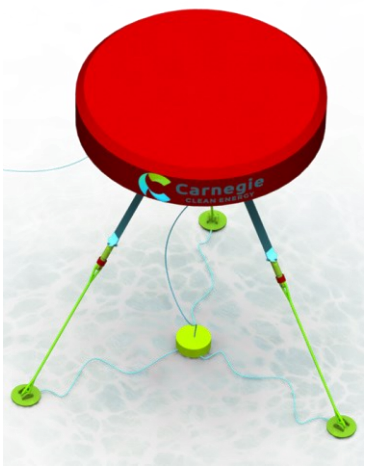

Fig. 1. The three-tether wave energy converter, CETO.

beyond locking the device in place where the hull of the WEC is still exposed to the large wave loads.

This is a critical aspect that needs to be addressed, especially as WECs are deployed in more challenging environments and at larger scales. Understanding the survivability of WECs can help to optimize their design and operation, reduce the risk of downtime and maintenance costs, and increase the confidence of investors and stakeholders. In this work, the fundamental challenge of wave energy will be tackled be substantially reducing the peak to average design parameters.

As seen in Fig. 1. CETO is a submerged three tethered WEC capable of being wound down in order to bring the device further away from the surface to reduce the hydrodynamic loads caused by the extreme waves on the surface. While the device's depth is increased, the PTOs

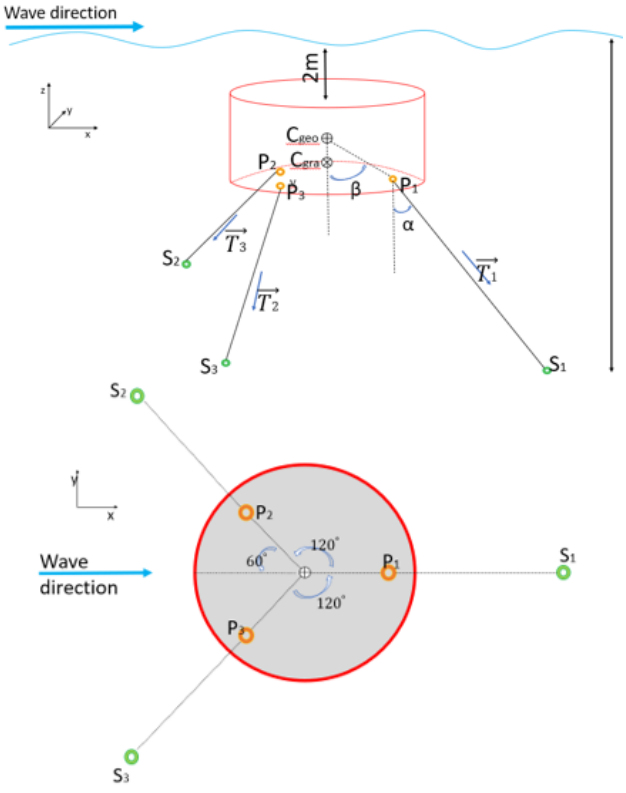

Fig. 2. A schematic of CETO

are tuned to minimize the dynamic response of the tethers/device instead of optimising energy production. These two mechanisms aim to keep the operation of the system in survival condition within the operational requirements. The main objective is to minimize the tether extensions in order to keep the device in place and maintain the integrity of the tethers PTOs.

This paper aims to analyse the state-of-the-art survivability technics. The paper will provide a case study of a WEC system deployed in a harsh marine environment at EMEC and evaluate its survivability and performance. Numerical simulations are carried out to check if this survival strategy is sufficient to maintain the operational conditions under extreme waves. Finally, scaled-down wave tank testing was conducted to check the viability of both survivability techniques.

The results of this study will contribute to the knowledge and understanding of WEC survivability and inform the design and deployment of future WEC projects.

It should be noted that most of the results presented in this paper are dimensionless due to commercial reasons.

II. THEORY AND MATHEMATICAL FORMULAE

Fig. 2. Shows a schematic of the three tethered WEC, CETO. It's a submerged three tethered cylinder. The three tethers are connected to the sea floor from one end, and to the BA (buoyant actuator) through three PTOs (Power Take-Offs) from the other end. The BA has an offset between the Cgrav (Centre of Gravity) and the Cgeo (Centre of geometry, which coincides with the centre of buoyancy) to maintain pitch stability. The WEC is a 6 DOF (Degrees Of Freedom) device. Applying Newton's second law with Cummins equation results in:

$$\sum_{j=1}^{6}\left(M_{ij}+A_{ij}^{\infty}\right)\ddot{x}_j+\int_{-\infty}^{t}K_{ij}(t-\tau)\dot{x}_j(\tau)\,d\tau = F_i^{wave}(t)+F_i^{pto}(t,\boldsymbol{x},\dot{\boldsymbol{x}}) + F_i^{buoyancy} + F_i^{Viscous\ Drag}(t) \quad (1)$$

Where the subscripts i and j represent the degree of freedom where 1 represents surge, 2 represents sway, 3 represents heave, 4 represents roll, 5 represents pitch and 6 represents yaw. x_j , $\dot{x}_j$ *and* $\ddot{x}_j$ represent the position, velocity, and acceleration of the device respectively. M_{ij} is the physical mass and inertia matrix. A_{ij}^{∞} is the added mass matrix. The convolution integral on the left-hand side of the equation represents the radiation fluid memory effects exerting on the system. $F_i^{wave}(t)$ is the time dependant wave excitation force acting on the system, $F_i^{pto}(t,\boldsymbol{x},\dot{\boldsymbol{x}})$ is the PTO (Power Take-Off) forces acting on the system through the three legs, and $F_i^{buoyancy}$ is the total buoyancy force resulting from the difference between the weight and the buoyancy force. $F_i^{Viscous\ Drag}(t)$ is the viscous drag

force acting on the device. The hydrodynamic coefficients are simulated using the open-source software Nemoh.

The viscous drag acting on the system is estimated based on the Morison equation:

$$F_i^{Viscous\ Drag}(t) = \frac{1}{2}\rho.C_{di}.A_{ri}.\dot{x}_i.|\dot{x}_i| \tag{2}$$

ρ is the density of water, A_{ri} is the cross-sectional reference area in the desired direction, and C_{di} is the non-dimensional viscous drag coefficient, calculated using three dimensional, RANS simulations.

In the RANS simulations, the drag coefficient is estimated separately in each degree of freedom. Basically, the BA is placed in a numerical water basin and oscillated in the specific degree of freedom under different frequencies and amplitudes of oscillations. The fluid forces acting on the oscillating BA are:

$$F^{fluid}(t) = \rho.V.\ddot{x} + \rho.C_a.V(\ddot{x} - \dot{u}) + \frac{1}{2}\rho.C_{di}.A_{ri}.(\dot{x} - u).|\dot{x} - u| \tag{3}$$

Where u is the velocity of the water particles, $\dot{u}$ is the acceleration of the fluid particles, V is the external volume of the BA and C_a is the hydrodynamic added mass coefficient. The first term of the fluid forces acting on the BA, $\rho.V.\ddot{x}$, is the Froude–Krylov force. The second term of the fluid forces, $\rho.C_a.V(\ddot{x} - \dot{u})$, is the hydrodynamic inertia force. The last term, $\frac{1}{2}\rho.C_{di}.A_{ri}.(\dot{x} - u).|\dot{x} - u|$, is the viscous drag force. Assuming the water particles velocity is negligible compared to the velocity of the BA, and evaluating the equation at points where the acceleration is zero to reduce the complexity, the viscous drag force coefficient is:

$$C_{di} = \frac{F^{fluid}(t_o)}{\frac{1}{2}\rho.C_{di}.A_{ri}.(\dot{x}).|\dot{x}|}\ at\ the\ instants\ t_o\ where\ \ddot{x} = 0\ . \tag{4}$$

The strategy for calculating the PTO force was adapted from [14] but derived for an arbitrary PTO location. It considers the geometry and notation established in Fig. 2. The attachment point of each tether at any instance in time is given by:

$$\boldsymbol{P_m}(t) = \boldsymbol{X}(t) + \boldsymbol{R}(t)\,\boldsymbol{P_m^0} \tag{5}$$

where $\boldsymbol{X}(t) = (x_1, x_2, x_3)^T$ is the instantaneous displacement of the BA's centre of gravity, $\boldsymbol{P_m^0}$ is the attachment point when the body is at rest, and: $\boldsymbol{R}(t)$ is the 3x3 rotation matrix. We define a vector that connects the tether from the BA to the seabed as

$$\boldsymbol{T_m}(t) = \boldsymbol{S_m} - \boldsymbol{P_m}(t) \tag{6}$$

$\boldsymbol{S_m}$ is the coordinates vector of the seabed anchoring points S1, S2 and S3. In this form the change in length of the tether, and the rate of change of this length, is defined as

$$\Delta L_m = |\boldsymbol{T_m}| - L_m \tag{7}$$

$$\begin{aligned}\Delta\dot{L}_m = \frac{\partial}{\partial t}|\boldsymbol{T_m}| &= (\boldsymbol{T_m}.\boldsymbol{T_m})^{-\frac{1}{2}}\boldsymbol{T_m}.\left(\frac{\partial}{\partial t}\boldsymbol{T_m}\right) \\ &= (\boldsymbol{T_m}.\boldsymbol{T_m})^{-\frac{1}{2}}\boldsymbol{T_m}.\left(\dot{\boldsymbol{X}} + \dot{\boldsymbol{R}}\,\boldsymbol{P_m^0}\right)\end{aligned} \tag{8}$$

respectively, where $L_m = |\boldsymbol{S_m} - \boldsymbol{P_m^0}|$ is the undeformed length of the mth tether and the dots denote the dot product. By considering the line of action of each tether, assuming that the PTO force function is a spring damper, the force and moments of the mth tether can therefore be defined as

$$\boldsymbol{F}_m = \left(C_m + K\Delta L_m + B\Delta\dot{L}_m\right)\frac{\boldsymbol{T}_m}{|\boldsymbol{T}_m|} \tag{9}$$

$$\boldsymbol{M}_m = (P_m - X) \times \boldsymbol{F}_m \tag{10}$$

where C_m is the pre-tensioning in the tether, K is its spring coefficient, and B is its dampening coefficient.

The total force from the PTOs is therefore given as

$$\boldsymbol{F}^{pto}(t, \boldsymbol{x}, \dot{\boldsymbol{x}}) = \sum_m \begin{bmatrix}\boldsymbol{F}_m \\ \boldsymbol{M}_m\end{bmatrix} \tag{11}$$

which can be calculated at an arbitrary timestep. In practice, the PTO force function is more complicated, and is split into two components, a mechanical spring component and a generator component:

$$\boldsymbol{F}_m = (F_{Tether})\frac{\boldsymbol{T}_m}{|\boldsymbol{T}_m|} = \left(F_{Mechanical\ Spring} + F_{Generator}\right)\frac{\boldsymbol{T}_m}{|\boldsymbol{T}_m|} \tag{12}$$

$F_{Mechanical\ Spring}$ is the mechanical spring force and composes both the pretension in the spring and a mechanical stiffness component:

$$F_{Mechanical\ Spring} = C_m + K_{Mech}\Delta L_m \tag{13}$$

This force is set to always be positive to avoid slacking in the lines. As for the generator force, this is typically the control force applied to the system, and can vary from a spring damper, to an MPC based control algorithm, to an AI based control force. This control force is provided by the generator and is usually limited to the maximum force and power the generator can handle.

$$-F_{Gen\ Max} < F_{Generator} < F_{Gen\ Max} \tag{14}$$

$$-\left|P_{Gen\ Max}/\Delta\dot{L}_m\right| < F_{Generator} < \left|P_{Gen\ Max}/\Delta\dot{L}_m\right| \tag{15}$$

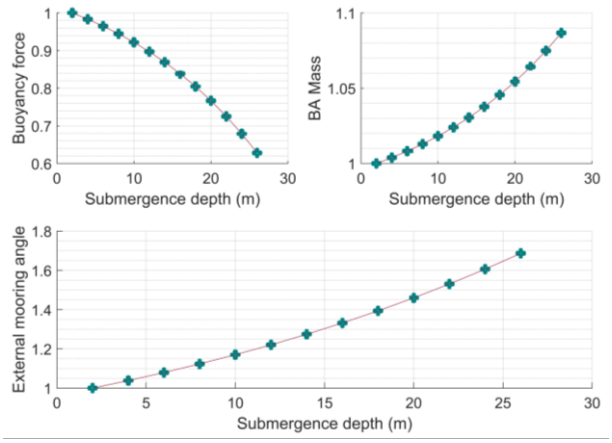

Fig. 3. The change of the external mooring angle and the mass and buoyancy of the BA with the increase of the submergence depth of the BA. All values are normalized to the values at operational submergence depth.

Where $F_{Gen\ Max}$ is the limit of the generator force, and $P_{Gen\ Max}$ is the limit of the generator power. These are usually determined from the specification sheet of the generator. F_{Tether} is also maintained between limits. Usually, it's kept always positive to avoid slacking in the line and capped at twice the value of the pretension C_m in order to maintain symmetry in the tether force around C_m. The tether force is usually maintained between the limits with the control force $F_{Generator}$ since it's difficult to control the mechanical spring force.

III. PROBLEM FORMULATION

CETO will be simulated at different depths to search for an optimal depth where the system response can be brought back to the maximum operational one. Dropping the device down results in altering its hydrodynamic entities, mainly reducing the wave excitation forces, the added mass and radiation damping entities. Also, dropping the device down using the tethers changes the external mooring angle as seen in Fig. 3. and hence the pretension requirement in the lines changes and a mechanism which deals with this change must be implemented as well. It should be noted that CETO is designed in a way where the weight force is lower than the upwards buoyancy force acting on it due to the displacement of the volume of water. The tethers have a constant pretension force to maintain the neutral position of the device. The reasoning behind this is to keep the tethers tight. CETO has ballast tanks which can pump water inside and outside the BA (Buoyant Actuator) in order to alter its mass to compensate for the reduction in the effective vertical component of the PTO pretension. This can be seen in the upper part of Fig. 3. Where the dry mass of the BA increases with the increase of depth, tether angle, resulting in a decrease in the buoyancy force acting on it as the buoyancy force is the weight force of the device subtracted from the upwards vertical force resulting from the displacement of the volume of water. In this work, the depth of the device was altered from 2 m to 26 m with 2 m increments. Different linear hydrodynamic simulations were conducted in Nemoh for every depth and used as an input to the in-house LTD model.

The PTO is set up as a SD (Spring Damper) where the same PTO coefficients were set to the front and back legs to minimize the tether extensions. It should be noted that the PTOs were set as conventional spring dampers and their coefficients were assumed to be the same across all legs. Instead of setting the PTO force to maximise the power output, they are set to minimize the tether extensions in order to ensure minimum system response under the extreme waves.

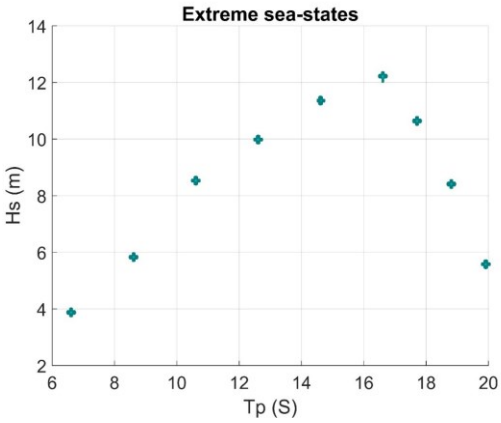

Fig. 4. Scatter plot of the extreme sea-states used in this work

The extreme sea-states used were related to the 50 years return storm from the EMEC site [13] and can be found in Table 1 and Fig. 4. The sea-states presented in Fig. 4. Represent the sea-states that sit on the 50 year contour at EMEC which are presented numerically in Table 1.

Table 1: The extreme sea-states used in this work

SS	Hs (m)	Tp (s)
1	3.88	6.61
2	5.83	8.61
3	8.53	10.61
4	9.98	12.61
5	11.36	14.61
6	12.22	16.61
7	10.64	17.71
8	8.41	18.81
9	5.58	19.916

It should be noted that the significant value refers to a statistical parameter like the Significant wave height, as it's the mean of the highest third of the amplitudes. This was found a better metric to analyse results compared to evaluating the absolute maximum, as that can be an outlier point.

IV. SIMULATION RESULTS

Fig. 5. shows the normalised hydrodynamic coefficients for every depth. As expected, all the hydrodynamic entities decrease with the increase of depth. This doesn't necessarily translate to the device's response decreasing

with the increase of the depth. Even though the wave excitation force in the heave and surge directions decreases, the pitch wave excitation force increases at low wave frequencies. Also, the radiation damping and the added mass both decrease with the increase of the depth.
In this section, 13 depths are simulated going from 2m to 26m submergence depth with 2m increments. For every depth, and every sea-state, the optimal SD PTO coefficients which result in the minimum of the maximum significant tether extension across all three legs were derived.
Fig. 6. show the BA response for the three main DOFs (surge, heave, and pitch) normalised against the maximum operational.

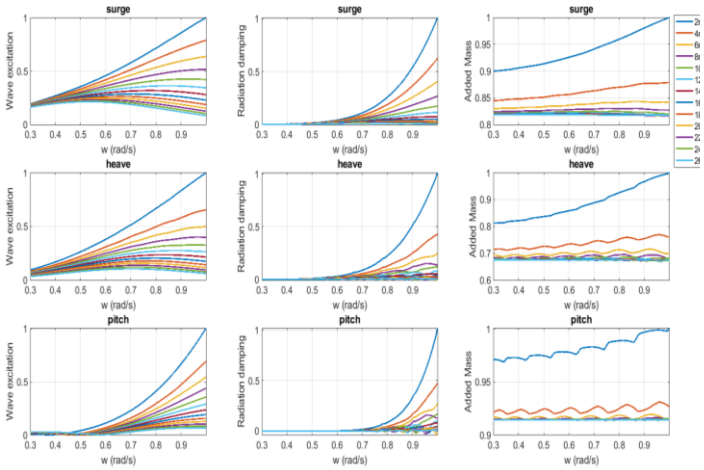

Fig. 5. The normalised linear hydrodynamic coefficients of the BA at different depths.

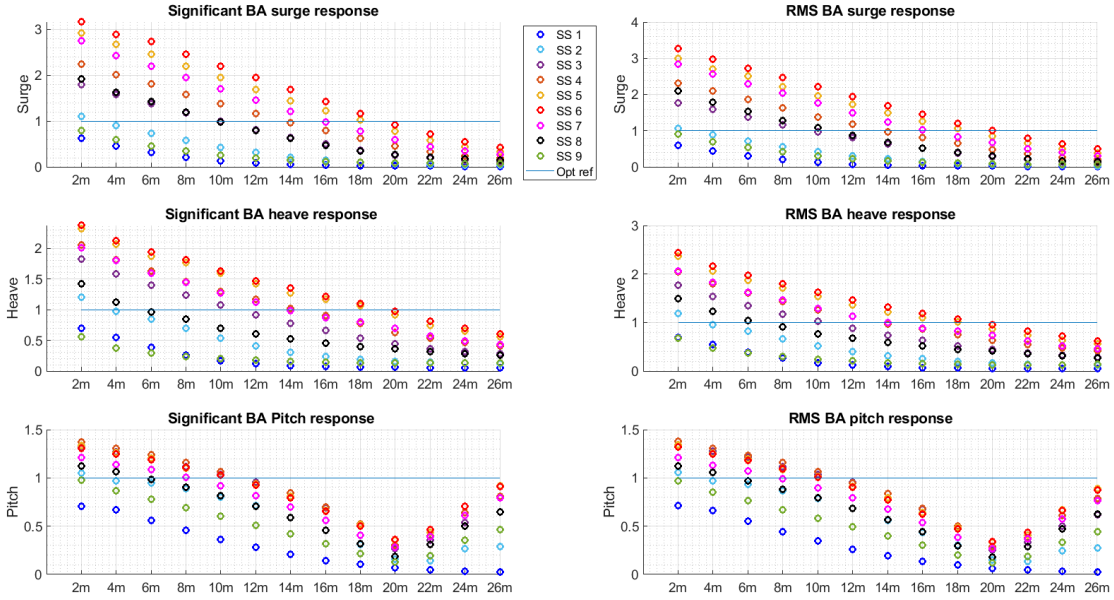

Fig. 6. The normalised BA response at different submergence depths

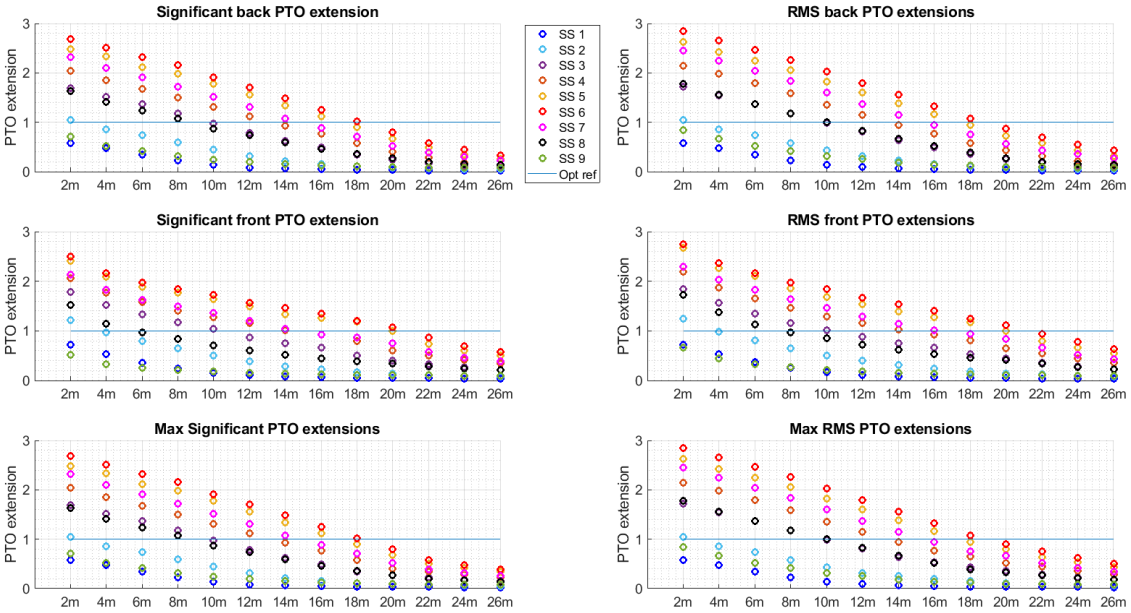

Fig. 7. The normalised PTO extensions at different submergence depths

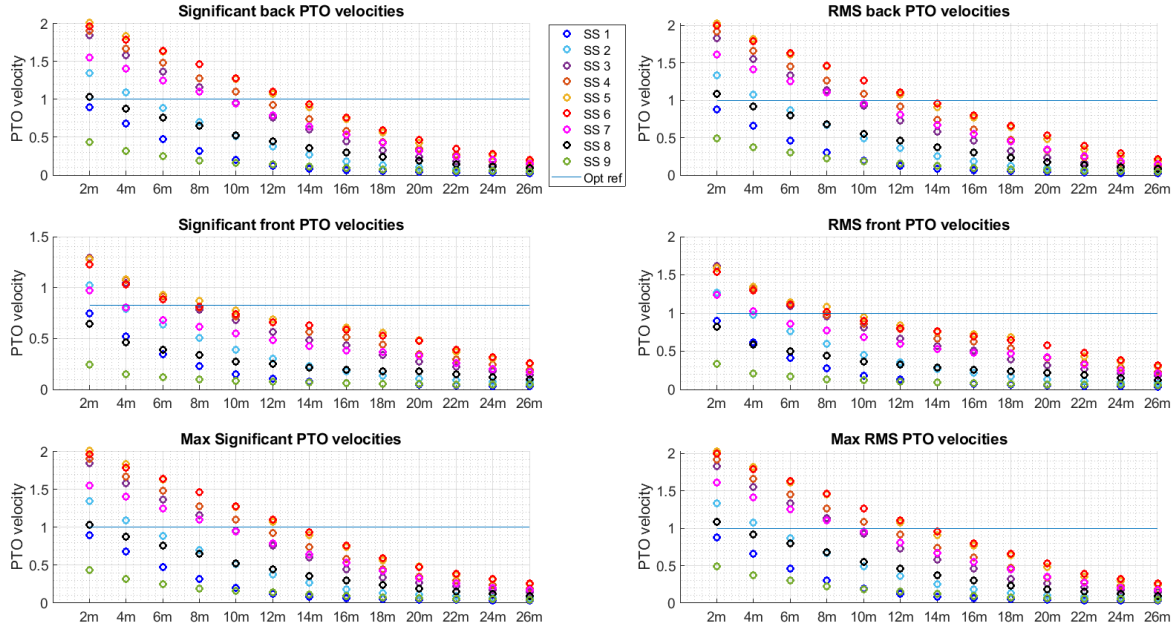

Fig. 8. The PTO velocities at different submergence depths

Fig. 6. show the statistical values of the PTO response normalised against the maximum operational. Fig. 7. show the statistical values of the PTO velocities normalised against the maximum operational. The operational design value, set at 4m maximum significant wave height in operational conditions is shown in a blue line. Fig. 8 shows the statistical values of the PTO velocities normalised against the operational maximum.

From a design perspective, the most important parameter to consider is the tether extensions. As seen in the previous section, The PTO of CETO includes a power and forces limiters that don't allow the PTO and generator forces and power to exceed certain limits to prevent a failure of the tethers, PTO, or generator. However, the PTO controller does not have a large authority over the PTO extensions, and therefore it is of high importance in this work as exceeding the PTO extensions will increase design requirement and thus cost. In general, almost all the parameters, at all the buoyancy levels, decrease with the increase of the submergence depth. One exception is the pitch response of the device, where it starts increasing at submergence depth levels larger than 20m. While increasing the submergence depth, the tether angle increases as seen in Fig. 3. This change of tether angle reduces the pitch component of the tether forces, hence reducing the damping in the pitch direction and resulting in an increase of the pitch response at large depths. Looking at both the max RMS and significant values of the PTO extensions, the BA should be submerged to a depth of 20m to mitigate the responses back to the operational maximum. Fig 8. suggests that the PTO velocities require even a smaller submergence depth in order to mitigate the PTO velocity back to the maximum operational, further emphasizing the previous suggestion that the tether extensions are the most important metric in this study.

It should also be noted that taking the device down to more than 20 m depth is only required for SS 5 and 6, as the other sea-states only require a submergence depth of around 14m in order to mitigate the response back to the operational maximum. SS5 and 6 are the sea-states with the larges Hs, and hence it seems that the maximum response at these extreme sea-states is driven by the wave height and not the wave period or a related resonance phenomenon.

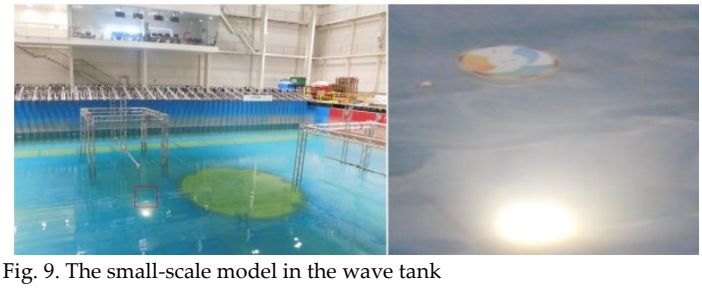

Fig. 9. The small-scale model in the wave tank

Fig. 10. The wave PTO model

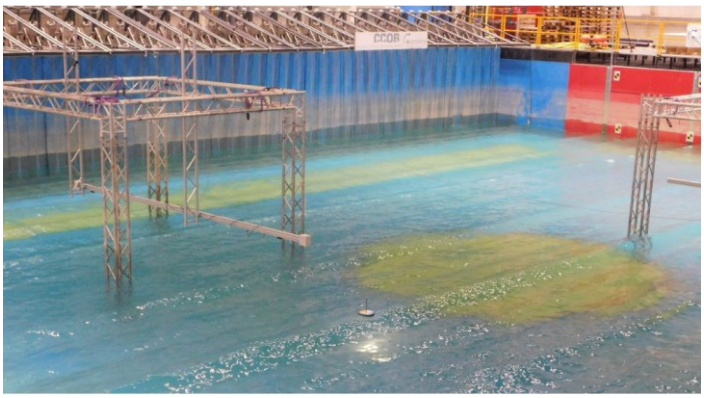

Fig. 11. The small-scale model operating in extreme waves in the wave tank

V. WAVE TANK SET-UP

A small-scale device was tested in the wave tank facility in IH Cantabria. The device had to be downscaled to 1:35 scale for the wave maker to be able to run waves with Hs=12.2m. Fig. 9. Shows the device in the wave tank. The three tethers are connected to the wave tank floor and then taken back outside the water through three pulleys. The tethers are then connected to three PTOs shown in Fig. 10. The PTOs attempt to provide the tether force from equation 12. Fig. 11. Shows CETO operating under a large wave with the operational submergence depth.

Table 2 shows the extreme sea-states tested in the wave tank facility. The sea-states are a combination of the most extreme waves representing the 50 year countour at EMEC from Table 1 and at the BiMEP (Biscaya Marine Energy Platform) [15]. The main objective of the tank testing is to showcase the validity of the survivability strategy.

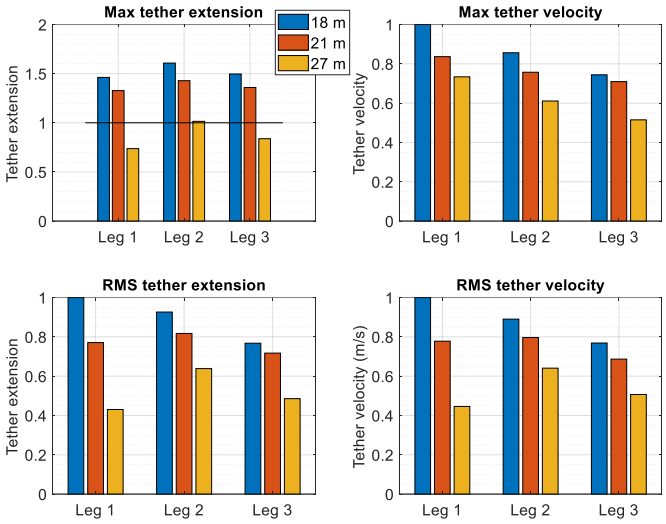

Fig. 12. The normalised tether responses for the three legs for three different submergence depths for ESS8

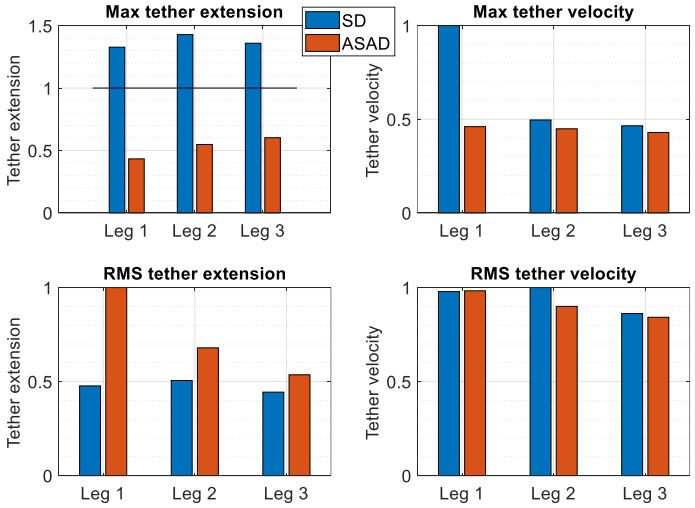

Fig. 13. The normalised tether responses for the three legs using the two different controllers for ESS8 and a submergence depth of 21m

Table 2: The sea-states tested in the tank

Sea-state	Hs (m)	Tp (s)
ESS1	3.9	6.6
ESS2	8.5	10.6
ESS5	12.2	16.6
ESS6	4.1	7.7
ESS7	8.9	14.2
ESS8	10.1	16.7
ESS9	10.2	18.0

VI. TANK TESTING RESULTS

First, the submergence effect is checked in the tank. Even though the numerical model suggested that submerging the device can mitigate its response greatly, in practice things might differ. The numerical results were based on BEM (Boundary Element Method) hydrodynamic simulations which don't account for the higher order hydrodynamic loads and viscous drags present on the BA, especially during large waves [8], [9].

Fig. 12. shows the tether extensions response for the three legs of CETO for three different submergence depths. The sea-state used is ESS8, and in the tank results, the statistical significant value can be replaced with the maximum as the tank model does not include numerical outliers. Also, it should be noted that the maximum extensions only refer to the extensions and excludes the minimums, as from a design perspective, the minimum tether retraction is not very relevant, whether the extension is of high importance as it is directly related to the design of the mechanical tensioner and the generator. Considering that the PTO controller has tether and force limiters, the maximum tether extension is the most important metric to be considered in these results. Fig. 12. Demonstrates how submerging the device down results in the reduction of the tether extensions of the device for both the maximum and the RMS. It is seen in the top left corner of Fig. 12, which is normalised against the maximum operational seen as a black line, that the device needs to be submerged to 27m depth in order to mitigate the response back to the operational maximum for ESS8. However, the numerical simulations suggested a negative spring coefficient and a large damping coefficient for the SD controller to mitigate the responses. These coefficients couldn't be achieved in the tank due to the downscaled PTO. The spring coefficient had to be set positively and the damping coefficient had to be set to around 60% of what the numerical model optimisation suggested. Hence the controller was not properly optimised. To get around this, the controller was altered to a modified SD, aimed to minimise tether extensions, uses an Asymmetrical Damper and Absolute Spring (ASAD). The electrical spring force is set to add to the mechanical spring during extension and subtract from it (effectively acting as a negative spring) during retraction. The damping is set to only damp when the tethers are extending, and not during retraction. The difference between the two controllers is apparent, as the ASAD controller results in a considerable reduction in the maximum tether extension and velocity across the three legs, which are some of the most cost impactful parameters. Fig. 13. shows the tether response for the three legs using both controllers for the same sea-state, ESS8. The reduction is in the range of 67-70% across the three legs. The maximum of the tether velocities is reduced by 8-16% across the three legs using the ASAD controller. Of less significance to CAPEX, the RMS of the tether extensions across the three legs increases going from the SD controller to the ASAD controller. The RMS of the tether velocities slightly increases for legs 2 and 3 going from the SD controller to the ASAD controller and the RMS of the tether velocities for leg 1 slightly increases going from the SD controller to the ASAD controller. It is seen from the top left corner of Fig. 13 where the results are normalised against the maximum operational, and the

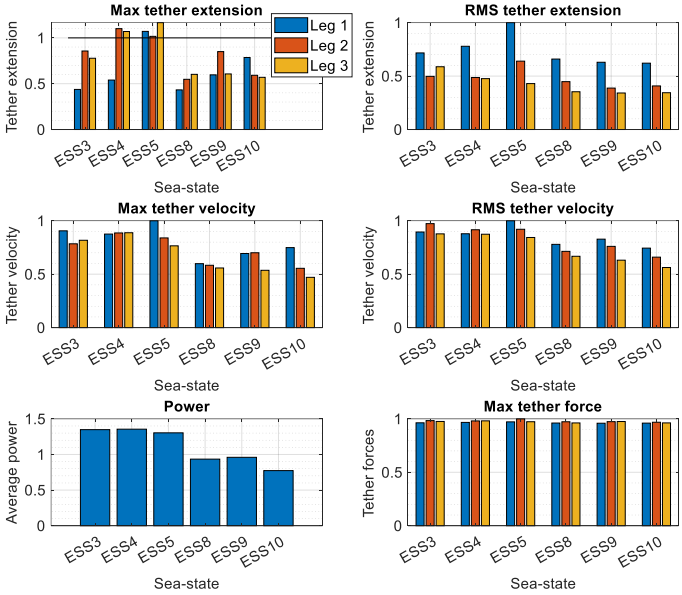

Fig. 14. The normalised system response for all the extreme sea-states for a submergence of 21m

maximum operational is plotted as a line, that the ASAD controller is capable of mitigating the system response back to the operational maximum for a depth of 21m, confirming the numerical model's prediction from the previous sections. Fig. 14. Shows all the system tether extensions, velocities, forces, and power for all the three legs, and all the tested sea-states for a submergence depth of 21m and using the ASAD modified controller. All the results are normalised against the maximum except for the maximum tether extensions which are modified against the maximum operational and the average power, which is normalised against the annual average power of CETO for the same scale, in order to check whether the device is drawing or making power in order to mitigate the response from one and to check the magnitude of the power. It is seen that the survivability strategy is successful in mitigating the system response at ESS3, ESS8, ESS9, and ESS10 when the device is taken down to 21m submergence depth. However, in ESS4 and ESS6, the operational maximum was exceeded by 10 to 16%. This can be due to the small-scaled PTO not operating efficiently due to the phase lag caused by the testing equipment. However, exceeding the system responses by 10-16% is acceptable in terms of design, where the design targets can be slightly increased to accommodate the survivability strategy. It should also be noted from Fig. 14 that the device is making power in the same magnitude as the average operational power while mitigating the system response in the extreme conditions. Lastly, it is seen from the lower right corner of Fig. 14. That the tether force is almost the same for all the tested sea-states. This is to showcase that the controller is obeying the tether force limits.

VII. CONCLUSIONS

In this paper, a survival strategy for the CETO WEC is proposed, numerically simulated, and tested in a wave tank. It was shown from numerical simulations that increasing the submergence depth of the device and altering the controller can successfully mitigate the system response back the operational maximum when the device is submerged to 21m depth. The wave tank tests showcased that the device only exceeds the operational limits by a maximum of 16% when submerged to a depth of 21m and using a modified controller. It was also shown that the device can still make power in the magnitude of its average operational power production.

The survivability strategy was shown that the design limits are only exceeded by 16% under the loads of a wave of Hs 12.2m compared to the maximum operational conditions that are simulated for a maximum Hs of 4m.

REFERENCES

[1] E. Al Shami, R. Zhang, and X. Wang, "Point Absorber Wave Energy Harvesters: A Review of Recent Developments," Energies (Basel), vol. 12, no. 1, 2019, doi: 10.3390/en12010047.

[2] D. Clemente, P. Rosa-Santos, and F. Taveira-Pinto, "On the potential synergies and applications of wave energy converters: A review," Renewable and Sustainable Energy Reviews, vol. 135, p. 110162, 2021, doi: https://doi.org/10.1016/j.rser.2020.110162.

[3] Y.-H. Yu, J. Van Rij, R. Coe, and M. Lawson, "Preliminary Wave Energy Converters Extreme Load Analysis," in Volume 9: Ocean Renewable Energy, American Society of Mechanical Engineers, May 2015. doi: 10.1115/OMAE2015-41532.

[4] S. J. Edwards and R. G. Coe, "The Effect of Environmental Contour Selection on Expected Wave Energy Converter Response," Journal of Offshore Mechanics and Arctic Engineering, vol. 141, no. 1, Aug. 2018, doi: 10.1115/1.4040834.

[5] B. Drew, A. R. Plummer, and M. N. Sahinkaya, "A review of wave energy converter technology," Proceedings of the Institution of Mechanical Engineers, Part A: Journal of Power and Energy, vol. 223, no. 8, pp. 887–902, Dec. 2009, doi: 10.1243/09576509JPE782.

[6] A. F. de O. Falcão, "Wave energy utilization: A review of the technologies," Renewable and Sustainable Energy Reviews, vol. 14, no. 3, pp. 899–918, Apr. 2010, doi: 10.1016/j.rser.2009.11.003.

[7] R. Coe, Y.-H. Yu, and J. van Rij, "A Survey of WEC Reliability, Survival and Design Practices," Energies (Basel), vol. 11, no. 1, p. 4, Dec. 2017, doi: 10.3390/en11010004.

[8] W. Chen et al., "Numerical modelling of a point-absorbing wave energy converter in irregular and extreme waves," Applied Ocean Research, vol. 63, pp. 90–105, Feb. 2017, doi: 10.1016/j.apor.2017.01.004.

[9] L. Sjökvist, J. Wu, E. Ransley, J. Engström, M. Eriksson, and M. Göteman, "Numerical models for the motion and forces of point-absorbing wave energy converters in extreme waves," Ocean Engineering, vol. 145, pp. 1–14, Nov. 2017, doi: 10.1016/j.oceaneng.2017.08.061.

[10] E. J. Ransley, D. Greaves, A. Raby, D. Simmonds, and M. Hann, "Survivability of wave energy converters using CFD," Renew Energy, vol. 109, pp. 235–247, Aug. 2017, doi: 10.1016/j.renene.2017.03.003.

[11] E. Quon, A. Platt, Y.-H. Yu, and M. Lawson, "Application of the Most Likely Extreme Response Method for Wave Energy Converters," in Volume 6: Ocean Space Utilization; Ocean Renewable Energy, American Society of

Mechanical Engineers, Jun. 2016. doi: 10.1115/OMAE2016-54751.
[12] V. S. Neary et al., "Characterization of Extreme Wave Conditions for Wave Energy Converter Design and Project Risk Assessment," J Mar Sci Eng, vol. 8, no. 4, p. 289, Apr. 2020, doi: 10.3390/jmse8040289.
[13] M. Folley, B. Elsaesser, and T. Whittaker, "Analysis of the wave energy resource at the European Marine Energy Centre," in Coasts, marine structures and breakwaters: Adapting to change, London: Thomas Telford Ltd, 2010, pp. 660–669. doi: 10.1680/cmsb.41301.0058.
[14] J. Orszaghova, H. Wolgamot, S. Draper, R. Eatock Taylor, P. H. Taylor, and and A. Rafiee, "Transverse motion instability of a submerged moored buoy," Proceedings of the Royal Society A: Mathematical, Physical and Engineering Sciences, vol. 475, no. 2221, p. 20180459, Jan. 2019, doi: 10.1098/rspa.2018.0459.
[15] H. Chiri, A. Cid, A. J. Abascal, J. García-Alba, A. García, and A. Iturrioz, "A high-resolution hindcast of sea level and 3D currents for marine renewable energy applications: A case study in the Bay of Biscay," Renew Energy, vol. 134, pp. 783–795, Apr. 2019, doi: 10.1016/j.renene.2018.11.069.